Molecular docking approaches to suggest the anti-mycobacterial targets of natural products

Rafael Baptista[1], Sumana Bhowmick[1], Shen Jianying[3, 2], Luis A. J. Mur[1,2*]

[1] Institute of Biological, Environmental and Rural Sciences, Aberystwyth University, Penglais Campus, Aberystwyth, Wales, UK, SY23 2DA.

[2] Artemisinin Research Center, Institute of Chinese Materia Medica, China Academy of Chinese Medical Sciences, Beijing 100700, China.

Correspondence: lum@aber.ac.uk; jyshen@icmm.ac.cn;

Abstract

Tuberculosis (TB) is a major global threat mostly due to the development of antibiotic resistant forms of *Mycobacterium tuberculosis,* the causal agent of the disease. Driven by the pressing need for new anti-mycobacterial agents, several natural products (NPs) have been shown to have *in vitro* activities against *M. tuberculosis*. The utility of any NP as a drug lead is augmented when the anti-mycobacterial target(s) is unknown. To suggest these, we used a molecular docking approach to predict the interactions of 53 selected anti-mycobacterial NPs against known 'druggable' mycobacterial targets ClpP1P2, DprE1, InhA, KasA, PanK, PknB and Pks13. The docking scores / binding free energies were predicted and calculated using AutoDock Vina along with physicochemical and structural properties of the NPs, using PaDEL descriptors. These were compared to the established inhibitor (control) drugs for each mycobacterial target. The specific interactions of the bisbenzylisoquinoline alkaloids 2-nortiliacorinine, tiliacorine and 13'-bromotiliacorinine against the targets PknB and DprE1 (-11.4, -10.9 and -9.8 kcal.mol^{-1}; -12.7, -10.9 and -10.3 kcal.mol^{-1}, respectively) and the lignan α-cubebin and Pks13 (-11.0 kcal.mol^{-1}) had significantly superior docking scores compared to controls. Our approach can be used to suggest predicted targets for the NP to be validated experimentally but these *in silico* steps are likely to facilitate drug optimisation.

Introduction

Tuberculosis (TB) is the leading cause of death from infectious diseases with 10 million new cases in 2017. About 1.7 billion people are estimated to have latent TB infection and therefore they are at risk of developing active TB disease during their lifetime [1]. The emergence of multidrug-resistant (MDR) and extremely drug-resistant (XDR) TB is primarily due to the improper use of the first line anti-tubercular drug. The increased prevalence of such strains has become a major obstacle in the treatment of TB and also a serious financial burden on the health care sector. As a result, there is an urgent need for new cost-effective anti-TB drugs with new mechanisms of action and less chance of developing resistances [2].

TB drug discovery has been based on the use of combinatorial chemistry and high-throughput screening strategies in drug discovery but recently, there has been an increased interest in plant based NP as drugs[2]. Plants are an important source of secondary metabolites which can have enormous therapeutic potential. They are still used in traditional medicine in such nations as China and in economically developing countries. Often, knowledge of medicinal plants is passed verbally from generation to generation without any proper documentation or scientific validation. However, medicinal plants still represent a resource that can be further explored for potential "hit" compounds with significant biological activity, i.e. drug leads [3]. These hit compounds are typically found in biochemically complex extracts and their identification can be considered to be equivalent to searching for a "needle in a haystack". This is usually approached through sequential rounds of bioassay informed purification but could be considerably accelerated if candidate chemicals could be screened against known and 'druggable' drug targets. Crucially, the identification of these targets facilitates drug optimisation for improved efficacy and such a reduced cytotoxicity [2].

Molecular docking is widely used to model interactions at the atomic level between a small molecule (ligand) and a known macromolecule[4]. Molecular docking and other bioinformatic tools represent cost-effective approaches to screen potential compounds prior to *in vitro* cell culture-based assays or chemical modifications to accelerate the overall drug discovery process. In this present study, we exploited the existing knowledge of anti-tubercular drug targets to predict the potential modes of action of NPs known to have activity against TB. Seven molecular targets of *M. tuberculosis* - ClpP1P2,

DprE1, InhA, KasA, PanK, PknB and Pks13 - were selected as these are essential for bacterial survival and their inhibition will affect mycobacterial metabolism[5]. We herein predict the binding of the NPs in comparison with the established inhibitor of the molecular target which was referred to as the control. We show that the specific interactions of the bisbenzylisoquinoline alkaloids 2-nortiliacorinine, tiliacorine and 13'-bromotiliacorinine against PknB and DprE1 and the lignan α-cubebin with Pks13 had significantly superior docking scores. The predicted interactions should facilitate the optimisation of the NP as a drug lead and beyond this establishes a strategy which could be applied to other NPs with any bioactivities.

Results

A total of 53 NPs with reported anti-mycobacterial activity (≤ 100 mg.mL^{-1}) were selected[3,6] (Table 1). These were subject to a series of *in silico* predictions to assess their "druggability" and suggest their targets. The 53 NPs were organised into chemical classes and then assessed for their individual binding energy against established anti-microbial target proteins; ClpP1P2, DprE1, InhA, KasA, PanK, PknB and Pks13 which were retrieved from Protein Data Bank (PDB). For ease of comparison, the binding energies associated to all groups of studied NPs against each mycobacterial target are given as box-plots and compared to the binding of the known anti-TB drug hit for each protein (Figure 1, control bindings are shown with a dashed line).

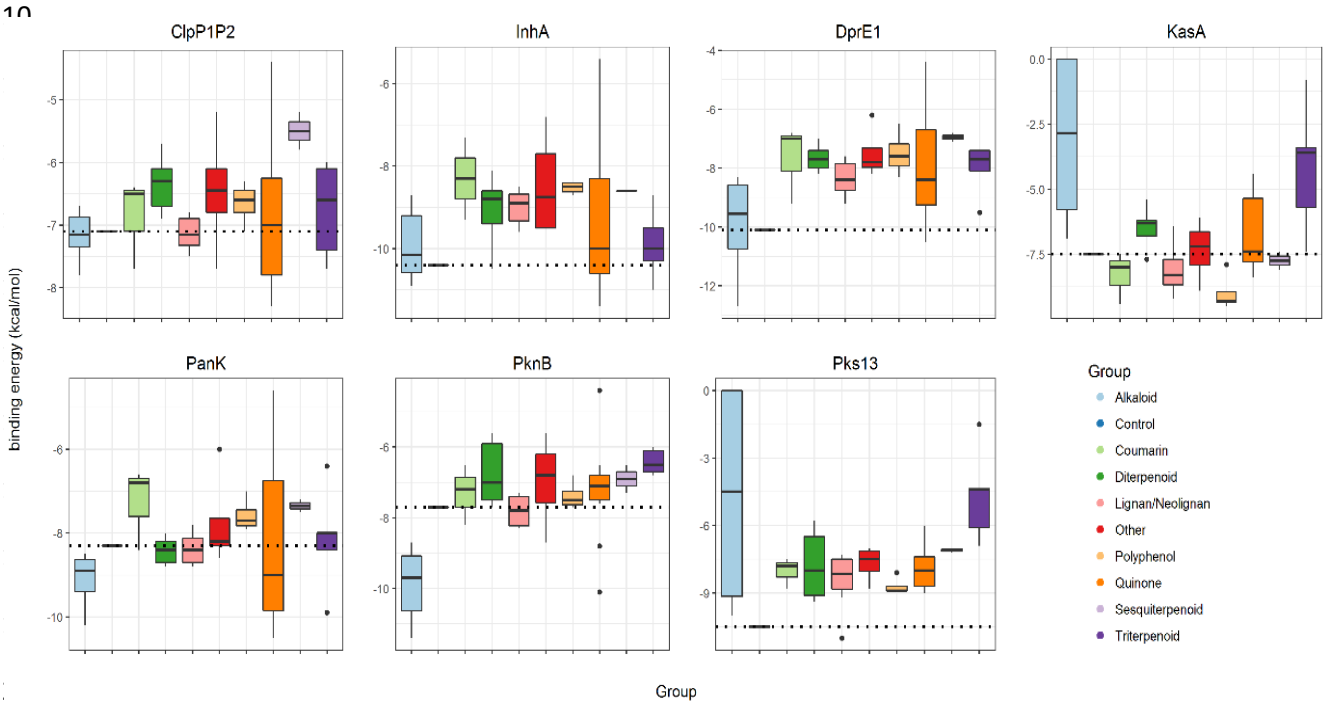

Figure 1 - Binding energies (kcal.mol^{-1}) of groups of selected natural products (alkaloids, coumarins, diterpenoids, lignans/neolignans, polyphenols, quinones, sesquiterpenoids, triterpenoids and others) and controls (represented with dashed lines) against mycobacterial targets ClpP1P2, InhA, DprE1, KasA, PanK, PknB and Pks13. Control inhibitors of each protein are, respectively, ZIL (N-[(benzyloxy)carbonyl]-L-isoleucyl-L-leucine), BTZ043 (bedaquiline), isoniazid, TLM (thiolactomycin), ZVT (2-chloro-N-[1-(5-{[2-(4-fluorophenoxy)ethyl]sulfanyl}-4-methyl-4H-1,2,4-triazol-3-yl)ethyl]benzamide), MIX (1,4-dihydroxy-5,8-bis({2-[(2-hydroxyethyl)amino]ethyl}amino)-9,10-antracenedione) and I28 (ethyl-5-hydroxy-4-[(4-methylpiperidin-1-yl)methyl]-2-phenyl-1-benzofuran-3-carboxylate).

Three targets, InhA, Pks13 and DprE1 exhibited poor binding to all of the studied NPs. Only a few alkaloids and quinones exhibited lower energies (-11.4 to -10.5 kcal.mol^{-1}) than the control drug

isoniazid (-10.4 kcal.mol^{-1}) against InhA. Considering Pks13, only one neolignan displayed a lower energy (-11.0 kcal.mol^{-1}) than the control drug I28 (ethyl 5-hydroxy-4-[(4-methylpiperidin-1-yl) methyl]-2-phenyl-1-benzofuran-3-carboxylate) (-10.5 kcal.mol^{-1}). Similarly, only alkaloids displayed favourable binding energies (-12.7 to -10.2 kcal.mol^{-1}), compared to the control, BTZ043 (bedaquiline) (-10.1 kcal.mol^{-1}) against DprE1. Indeed, it was mostly alkaloids, that exhibited very low binding energies (-11.4 to -8.7 kcal.mol^{-1}) against PknB, when compared with the control inhibitor MIX (1,4-dihydroxy-5,8-bis({2-[(2-hydroxyethyl)amino]ethyl}amino)-9,10-antracenedione) (-7.7 kcal.mol^{-1}). In contrast, KasA and ClpP1P2 were shown to have some binding energy to a wide range of natural product classes. For KasA and ClpP1P2, binding was seen with coumarins, lignans/neolignans, polyphenols and quinones. KasA is also bound by sesquiterpanoids and ClpP1P2, by triterpenoids. Although the PanK is predicted to bind to different classes of NPs, the alkaloids and quinones had lower binding energies (-10.5 to -8.5 kcal.mol^{-1}) compared with the control ZVT (2-chloro-N-[1-(5-{[2-(4-fluorophenoxy) ethyl]sulfanyl}-4-methyl-4H-1,2,4-triazol-3-yl)ethyl]benzamide) (-8.3 kcal.mol^{-1}).

The average of MW presented by conventional anti-TB drugs[7] (358.5 g.mol^{-1}) contrasted with our NPs that typically had lower binding energies (MW > 500 g.mol^{-1}). However, the number of H-bonds acceptors of the NPs matched those of H-bonds acceptors of conventional anti-TB drugs[7], the majority of which were below 10 H-bonds acceptors. The same is observed with the number of rotational bonds, since 88% of conventional anti-TB drugs have less than 10 rotational bonds[7].

PaDEL-Descriptor was used to assess the key physicochemical properties necessary for an optimal binding between the NP with ClpP1P2, DprE1, InhA, KasA, PanK, PknB and Pks13, compared to each respective control drug. PaDEL-Descriptor provided molecular weight (MW), partition coefficient (xLogP), rotatable bonds (nRotB), H-bond donors (nHBDon_Lipinski), H-bond acceptors (nHBAcc_Lipinski) and topological polar surface area (TopoPSA) (Supplementary Table 1). For ClpP1P2, InhA and PanK, there was a clear tendency for molecules with a higher topological polar surface area to have more favourable binding energies. This is due, in part, to the low binding energies of quinones against these three protein targets (Supplementary Figure 1). Higher MW appeared to have

lower binding energies against ClpP1P2, InhA, DprE1, PanK and PknB. In this higher MW category of natural product; lower binding energies, usually lower than the control inhibitor were mostly seen with triterpenoids and sesquiterpenoids (Supplementary Figure 2). When the lipophilicities of the NPs were analysed compared to binding energies, no particular tendency was observed (Supplementary Figure 3). The NP with more favourable binding energies did not exhibit distinctive partition coefficients as indicated by xLogP values. For PanK, DrpE1 and PknB, a higher number of H-bond acceptors (maximum of 8) was associated to lower binding energies. No similar trend was seen for the number of H-bond donors (Supplementary Figure 4 and 5). NPs with smaller rotation bonds were often linked to lower binding energies (Supplementary Figure 6).

Unsupervised principal component analysis (PCA) was used to provide a multivariate comparison of the physicochemical parameters of the selected NPs and 14 licensed anti-TB drugs (Figure 2). There was a large clustering of most NPs and anti-TB drugs suggesting a significant commonality of properties. However, six anti-TB drugs (isoniazid, ethambutol, streptomycin, kanamycin, amikacin and levofloxacin, large red circle in Figure 3) do not cluster with the NPs mainly due to their high hydrophilicity. The three aminoglycosides, streptomycin, kanamycin and amikacin also exhibit a high number of H-bonds donor ($n > 10$), which does not conform to one of "Lipinski's rule of five". Some NPs (selina-3, 7 (11)-diene, abietane and α-curcumene), represented in a large green circle in Figure 3, possessed distinctive chemical properties due to lack of any H-bond acceptors or donors. This would exclude them from being possible drug candidates without further derivatisation.

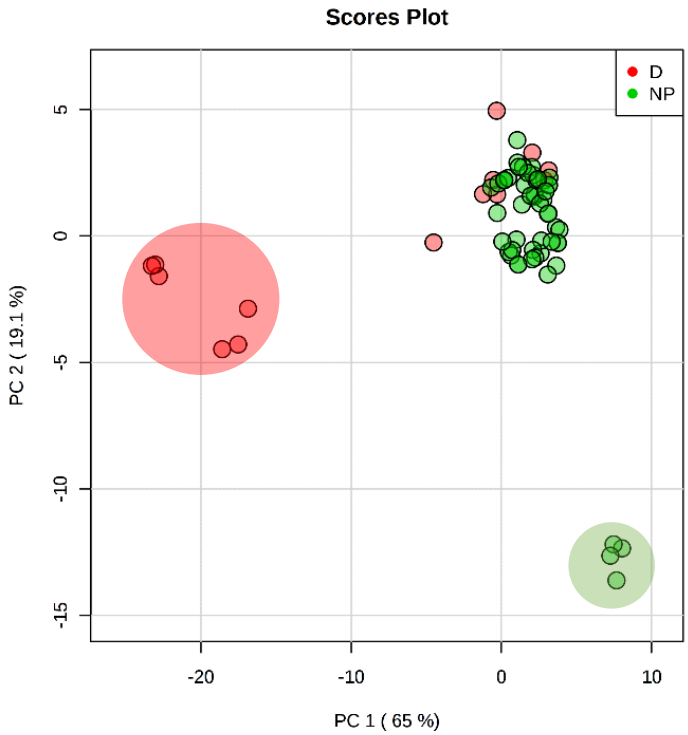

Figure 2 – PCA of the physicochemical parameters of 53 analysed natural products (NP) and 14 anti-TB drugs (D). In one cluster NP and D share similar physical and chemical properties but two other clusters are unique of D (red larger circle) and another for NPs (green larger circle).

Subsequently, a structural study was undertaken with the NPs that exhibited the most favourable anti-mycobacterial profiles i.e. show lower energies than the control inhibitor (Figure 1). Thus, the interaction between the bisbenzylisoquinoline alkaloids 2-nortiliacorinine, tiliacorine and 13'-bromotiliacorinine against the targets PknB and DprE1 were modelled.

The interaction of tiliacorine, nortiliacorinine and 13'-bromotiliacorine with PknB is shown in Figure 3 and exhibited binding energies of -11.4, -10.9 and -9.8 kcal.mol^{-1}, respectively. These values are significantly lower from the binding energy found for the control drug, MIX (-7.7 kcal.mol^{-1}). The best docking positions of each of the three NPs were compared and these showed considerable overlap (Figure 4). Such commonality of interaction could be related to inhibitory function and could guide drug optimisation. In particular, a key feature here revealed is the interactions of the hydrophobic core

of these NPs with PnkB[49] a feature also seen with the planar dihydroxy anthraquinone moiety of the control drug.

A B C

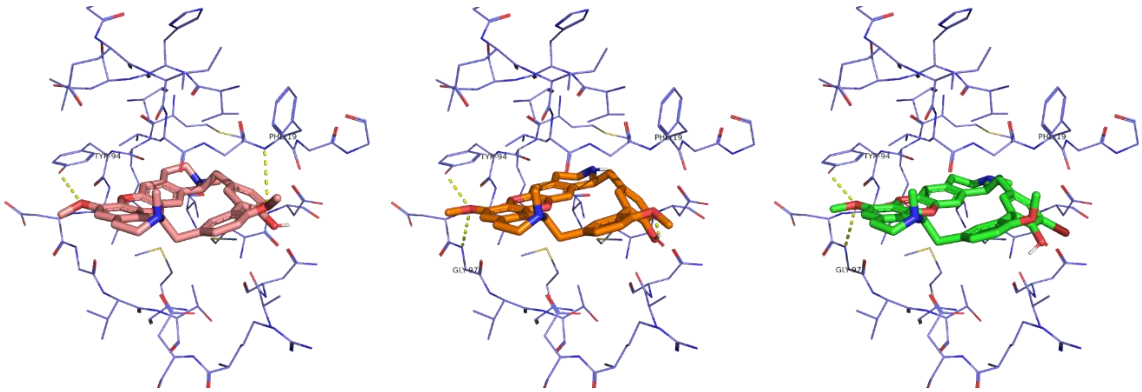

Figure 3 – Molecular interactions of the best docking positions of tiliacorine (A), nortiliacorinine (B) and 13'-bromotiliacorine (C) against PknB. Hydrogen bonds are shown as yellow dashed lines.

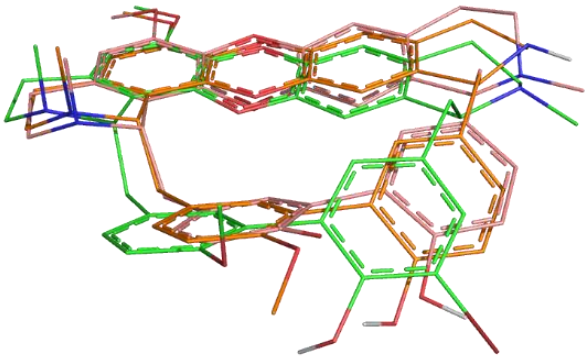

Figure 4 – Superposition of the best docking positions of tiliacorine (pink), nortiliacorinine (orange) and 13'-bromotiliacorine (green) against PknB.

The predicted interactions of tiliacorine, nortiliacorinine and 13'-bromotiliacorine with DprE1 were also visualised (Figure 5). Again, the interactions for all these NPs appeared to nearly superimpose. These showed better binding energies against DprE1, -12.7, -10.9 and -10.3 kcal.mol^{-1}, respectively than the benzothiazinethione drug control BTZ043 (-10.1 kcal.mol^{-1}). The binding of DprE1 to

tiliacorine, nortiliacorinine and 13'-bromotiliacorine, is stabilised by several non-covalent interactions. The LigPlot+ analysis shows that key van der Waals interactions with the residues Trp230, Val365, Lys367, Lys134, Tyr415, His132, Pro116, Ile131, Ala417, Lys418, Arg58, Thr118, Trp16, Tyr60, Gly117 and Tyr314 are responsible for the low binding energies of these structures with DprE1.

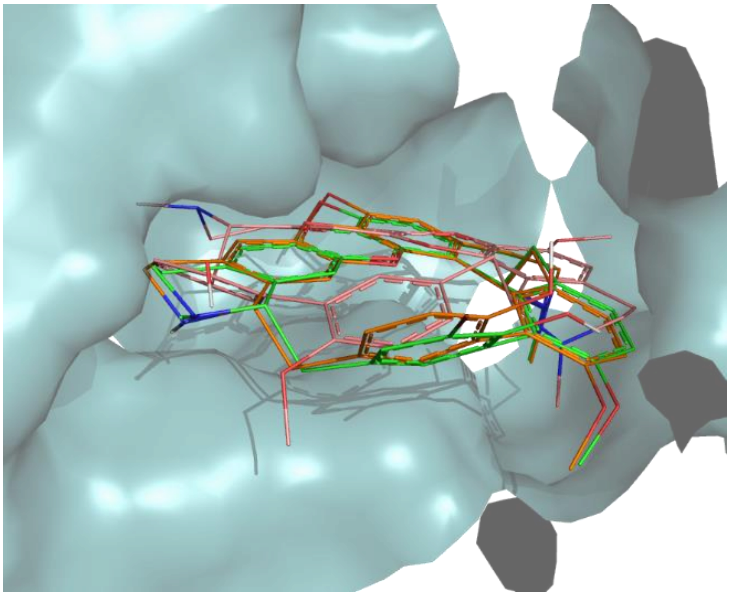

Figure 5 – Superposition of best docking position of tiliacorine (pink), nortiliacorinine (orange) and 13'-bromotiliacorine (green) against DprE1.

The interaction between the lignan α-cubebin and Pks13 was examined (Figure 6) as it had a lower docking scoring (-11.0 kcal.mol^{-1}) compared to the control I28 (-10.5 kcal.mol^{-1}). α-cubebin interacts with Pks13 via two H-bonds with the residues Asp1644 and Gln1633 and several hydrophobic interactions with the residues Tyr1637, Ser1636, Phe1670, Ile1643, Tyr1663, Tyr1674, Ala1667, Asn1640 and Arg1641. The interaction with the residues Tyr1663, Tyr1674, Asn1640, Asp1644 and Gln1633 are also key features in the binding of the control drug I28 against Pks13 [8].

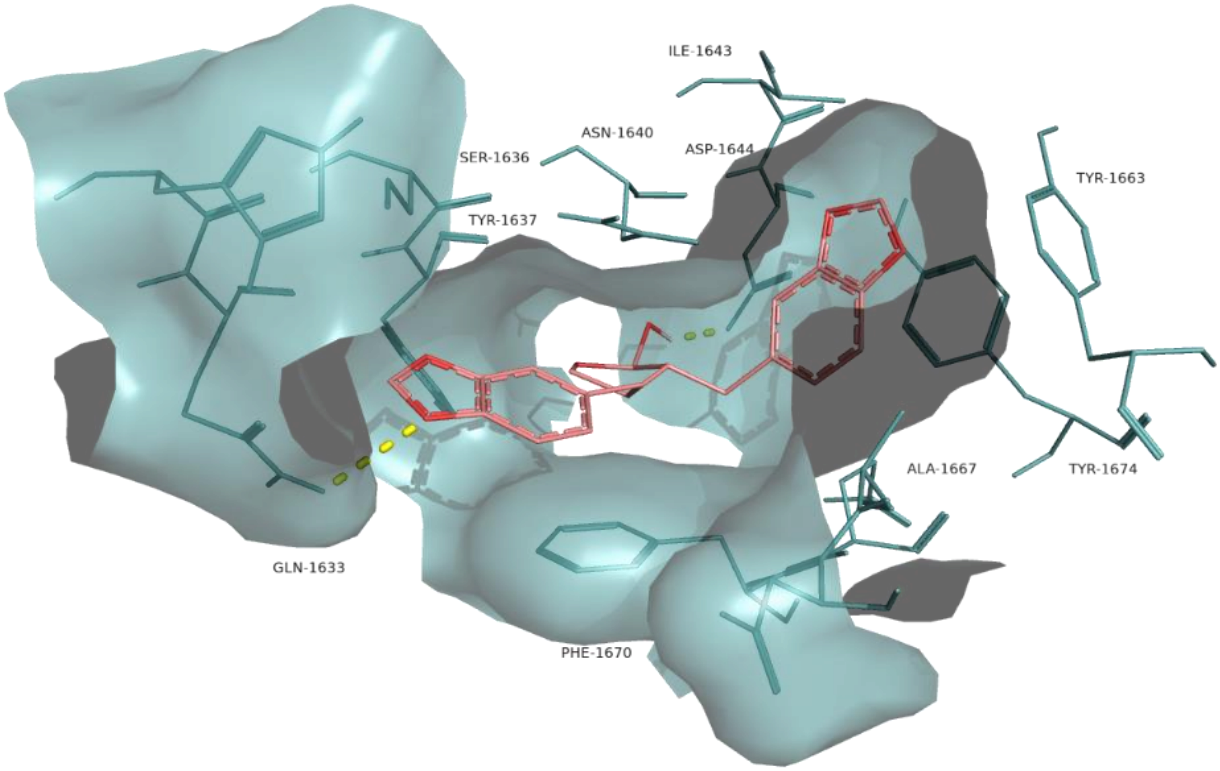

Figure 6 – Molecular interactions of the best docking position of α-cubebin against Pks13. Hydrogen bonds are evidenced with yellow dashed lines.

Discussion

Predictions of molecular docking are now well-established when assessing the interactions between ligands and targets. The use of docking approaches has been facilitated by the development of suitable software such as, GOLD, FlexX, FRED, DOCK and particularly, AutoDock Vina [9,10]. Such *in silico* docking provides a numerical estimate the likelihood of interaction of a compound to its target. This approach can be extended to identify the proteins which are likely *in vivo* binding sites, and therefore possible modes of action[11–13]. For example, the target of the anti-bacterial and anti-fungal natural product scytoscalarol was found to dock with EmbC and this was linked with anti-mycobacterial activity. Other compounds such as the β-carboline alkaloids 8-hydroxymanzamine A and manzamine A were found to bind to the oxidoreductase InhA.

We here demonstrate how docking can be used to assess large numbers of anti-mycobacterial NPs to suggest key interactions and imply a mode of action. Our approach was to examine the literature for

NPs with anti-mycobacterial activities but whose targets had not been previously characterised. Then, proteins known to be targeted by established anti-mycobacterial drug leads were screened using the NP chemical structures. The aim was to identify natural product interactions whose docking energies that were as good as, or superior to, the established drug lead. The 'druggable' mycobacterial targets ClpP1P2, DprE1, InhA, KasA, PanK, PknB and Pks13 were all known to play important roles in maintaining mycobacterial viability. ClpP1P2 carries out the energy-dependent degradation of abnormal proteins within the cells during *in vitro* growth and infection[14]. DprE1 is a decaprenylphosphoryl-d-ribose oxidase, involved in the biosynthesis of decaprenylphosphoryl-D-arabinose, an essential component of the mycobacterial cell wall and thus is essential for cell growth and survival[15,16]. InhA is a known target of isoniazid, a first-line anti-tuberculosis drug, essential for the synthesis of mycolic acids. KasA is one of the enzyme responsible for elongation of C16-26 fatty acyl primers in FAS-II system for mycolic acid production of *M. tuberculosis* [17]. Pantothenate kinase (PanK) is a ubiquitous and essential enzyme that catalyses the first step of the coenzyme A biosynthetic pathway[18]. PknB is a very well-characterized mycobacterial serine/threonine protein kinase which determines cell shape, morphology and possibly cell division[19]**.** Pks13 is a polyketide synthase that catalyses the final condensation step in mycolic acid biosynthesis and is therefore essential for mycobacterial growth [20].

A key aspect of our approach was to identify several "drug-like" properties of the NPs to by comparison conventional anti-TB drugs [7]. Our analyses first assessed the chemical space occupied by the NPs against ClpP1P2, DprE1, InhA, KasA, PanK, PknB and Pks13 which were compared with the respective control inhibitor. This identified NPs which occupied the same "chemical space" as most of the anti-TB drugs. Only isoniazid, ethambutol, streptomycin, kanamycin, amikacin and levofloxacin, exhibited a higher hydrophilicity compared to the NP. This could indicate that a few NPs have high cytotoxicity, due to their higher relative lipophilicity. This will have to be directly assessed through experimental testing.

Our structural study focused on bisbenzylisoquinoline alkaloids 2-nortiliacorinine, tiliacorine and 13'-bromotiliacorinine against the targets PknB and DprE1. These bisbenzylisoquinoline alkaloids isolated from *Tiliacora triandra* roots, which are used in Thai cuisine, were very effective in suppressing 59 isolated MDR-TB strains with MICs in the range of 1.5-6.25 µg.mL[1,21]. Structurally, these molecules are similar, but the minor differences resulted in different binding properties. Tiliacorine, with the lowest binding energy, formed two hydrogen bonds with the residues Tyr94 and Phe19 of PknB. However, both nortiliacorinine and 13'-bromotiliacorine only formed one stable hydrogen bond with Gly97 and Tyr94 (Figure 2). The bromide substitution at C-13 of 13'-bromotiliacorine made the molecule less planar and thereby increased the binding energy through steric impedance as seen with the superimposed docked conformations of all three molecules (Figure 3). A key feature here revealed is the interactions of the hydrophobic core of these NPs and the planar dihydroxy anthraquinone moiety of the control in the hydrophobic 'cage' of PnkB [22].

The importance of our modelling approach for drug optimisation was demonstrated by considering the binding of DprE1 to tiliacorine, nortiliacorinine and 13'-bromotiliacorine. The interaction with these NPs is stabilised by several non-covalent interactions but crucially, these were distinctive from the binding simulations with BTZ043, where H-bonding, hydrophobic and ionic interactions are responsible for the stabilisation of the complex[23]. Additionally, the residue Cys387, before identified as critical for covalently binding to Ct325 (3-(hydroxyamino)-N-[(1R)-1-phenylethyl]-5-(trifluoromethyl) benzamide) is not involved in the binding of any of the NPs. Overall, 13'-bromo-tiliacorinine have shown slightly better anti-mycobacterial activity (and lower cytotoxicity against MRC-5 cell lines) than tiliacorine, nortiliacorinine, despite the higher binding energies here reported. Other biochemical assays are required to understand the how the different chemical properties of these NPs influence bacterial uptake, metabolism and target binding. Nonetheless, the molecular interactions that we have defined can be used to inform chemical derivatisation strategies aiming to increase specificity and decrease toxicity.

α-cubebin, a dibenzylbutyrolactone lignan, has been isolated from several species in various families, such as Aristolochiaceae, Myristicaceae, Rutaceae, and Piperaceae [24]. It is known to act as an insect antifeedant as was noted with *Anticarsia gemmatalis* [25,26] as well as being anti-tubercular [27]. However, α-cubebin displays only a moderate activity against several mono- and multi-drug resistant isolates of *M. tuberculosis* (MICs ranging 50-100 $\mu g.mL^{-1}$). Interestingly, it does not display cytotoxicity against LLCMK2 fibroblast[28], suggesting that α-cubebin could merit derivatisation to make it a better drug lead. α-cubebin exhibited a low binding energy value when docked to Pks13 and interacts with some of the key residues within Pks13 as the drug inhibitor I28. Additionally, unlike I28, α-cubebin has been predicted to bind to the Protein Tyrosine Phosphatase B (PtpB) of *M. tuberculosis*[29]. This suggested that α-cubebin had some unique distinct binding characteristics with the *M. tuberculosis* proteome compared to 128. The information of α-cubebin's binding site will facilitate the optimisation of this compound towards greater efficacy and selectivity.

In conclusion, we show how four promising NPs - tiliacorine, nortiliacorinine, 13'-bromotiliacorine and α-cubebin - have very lower binding energies than the respective controls against three 'druggable' anti-mycobacterial targets PnkB, DprE1 and Pks13. Due to problems in obtaining the NPs from natural sources or complex total synthesis, the predicted *in silico* activity/binding will greatly facilitate drug optimisation prior to further studies. Even though the direct relation between *in silico* and *in vitro* results is not always correlated, our approach will generate hypotheses that should inform the discovery and synthesis of new and promising anti-TB derivatives based on docking models.

Materials and Methods

Selected anti-tubercular Natural Products

Information about the selected anti-mycobacterial NPs and their activity against TB, in minimum inhibitory concentration (MIC) is given in Table 1.

Table 1 - Plants and their molecules active against different *Mycobacterium* strains.

Plant names	Active phytomolecules	MIC (µg/mL)	References
Andrographis paniculata	Andrographolide	-	[30,31]
Aristolochia brevipes Benth.	6α-7-Dehydro-N-formyl-nornantenine	>50[a,b,d]	[32]
	N-Formylnornantenine	>50[a,b,d]	
	Aristolactam I	12.5–25[a,b,d]	
Aristolochia taliscana Hook and Arn.	Licarin A	3.12-25[a,b,d]	[33]
	Licarin B	12.5-5[a,b,d]	
	Eupomatenoid-7	6.25-50[a,b,d]	
Aristolochia elegans Mast.	Fargesin	12-50[a,b,d]	[27]
	(8R,8'R,9R)-Cubebin or α-Cubebin	50-100[a,b,d]	
Artemisia capillaris Thunb.	Ursolic acid	12.5-50[a,b,c,d]	[34,35]
	Hydroquinone	12.5-25 [a,b,c,d]	[35]
Azorella compacta Phil., A. madreporica Clos.	Azorellanol	12.5[b,d]	[36]
	Mulin-11,13-dien-20-oic acid	25-50[b,d]	
	Mulinol	12.5-25[b,d]	
Beilschmiedia tsangii Merr.	Beilschmin A	2.5[d]	[37]
Blepharodon nitidum (Vell.) J.F. Macbr.	25-Hydroperoxycycloart-23-en-3β-ol	25[b]	[38]
Citrullus colocynthis (L.) Schrad.	Cucurbitacin-E-2-*o*-β-d-glucopyranoside	25-62.5[a,b,c,d]	[39]
Clavija procera B.Ståhl	Aegicerin	1.6-3.12[a,b,d]	[40]
Curcuma longa L.	Curcumin	100[d]	[41]
	Demethoxycurcumin	50[d]	
	Bisdemethoxycurcumin	25[d]	
Diospyros anisandra S.F.Blake	Plumbagin	1.5-62.5[b,c,d]	[42,43]
	Maritinone or 8,8'-Biplumbagin	3.12[b,d]	[42]
	3,3'-Biplumbagin	3.12[b,d]	
Diospyros montana	Diospyrin	8-250[b,c,d]	[43,44]
Euclea natalensis A.DC.	7-Methyljuglone	0.5-1.25[a,b,d]	[44]
	Mamegakinone	100[d]	[45]
	Isodiospyrin	10[d]	
	Neodiospyrin	10[d]	
	Shinanolone	100[d]	
Ferula communis Linn.	Ferulenol	1.25[c]	[46]
Foeniculum vulgare Mill.	5-Hydroxy-furanocoumarin or Bergaptol	100-200[b]	[47]
Juniperus communis subsp. communis var. communis L.	Totarol	2-25[a,c,d]	[48]
	Ferruginol	5[c]	[49]
	Sandaracopimeric acid	30[c]	
	4-Epiabietol	60[c]	
Justicia adhatoda L. or *Adhatoda vesica*	Vasicine	200[d]	
Kaempferia galangal L.	Ethyl-*p*-methoxycinnamate	50-100[b,d]	[50]
Lantana hispida Kunth	Oleanolic acid	25-100[a,b,c,d]	[34,51]
Larrea tridentata Coville.	Dihydroguaiaretic acid	12-50[b,d]	[52]
	4-Epi-larreatricin	25-50[b,d]	
Plectranthus grandidentatus Gurke	Abietane	3.12-25[b,d]	[53]
Plumeria bicolor Ruiz & Pav.	Plumericin	1.5-2[b,d]	[54]
	Isoplumericin	2-2.5[b,d]	
Struthanthus concinnus	Obtusifoliol	50[d]	[55]

Tabernaemontana elegans Stapf. or *Tiliacora triandra*	Tiliacorinine	3.12-6.25[b,d]	21
	2'-Nortiliacorinine	1.5-6.25[b,d]	
	13′-Bromotiliacorinine	1.5-6.25[b,d]	
Ventilago madraspatana	Emodin	4-128[b,c]	43
Vetiveria zizanioides	α-Curcumene	31.25-125[a,b,c]	56
	Valencene	62.5-250[a,b,c]	
	Selina-3,7(11)-diene		

[a]mono-resistant clinical and non-clinical isolates, [m]ultidrug resistant (MDR) clinical and non-clinical isolates, [c]mycobacteria other than tuberculosis, [d]*Mycobacterium tuberculosis*

Ligand and Protein selection

A total of 53 NPs with reported anti-mycobacterial activity ≤ 100 mg.mL^{-1} were selected. All chemical structures were retrieved from the PubChem compound database (NCBI) (http://www.pubchem.ncbi.nlm.nih.gov). The crystal structures and respective controls of ClpP1P2 (PDB ID: 4U0G) [57], DprE1 (PDB ID: 6HEZ) [58], InhA (PDB ID: 1ENY) [59], KasA (PDB ID: 2WGE) [60], PanK type 1 (PDB ID: 4BFT) [61], PknB (PDB ID: 2FUM) [22] and Pks13 (PDB ID: 5V3X)[8] were retrieved from the RCSB Protein Data Bank (PDB) database (https://www.rcsb.org).

Physicochemical and structural properties

In silico prediction of physicochemical and structural properties of the NPs was performed using PaDEL-Descriptor[62] including the descriptors: nHBAcc_Lipinski (acceptor H-bonds), nHBDon_Lipinski (donor H-bonds), nRotB (number of rotation bonds), TopoPSA (topological polar surface area), MW (molecular weight) and XLogP (prediction of logP based on the atom-type method). Chemical space analyses were conducted with the NPs and 14 anti-TB drugs (ethambutol, isoniazid, pyrazinamide, rifampicin, streptomycin, ciprofloxacin, levofloxacin, moxifloxacin, amikacin, kanamycin, linezolid, bedaquiline, clofazimine and delamanid), comparing the descriptors above. Unsupervised principal component analyses (PCA) were generated using the statistical analysis tool of Metaboanalyst 4.0 [63].

Docking

The extended PDB format, PDBQT, was used for coordinate files to include atomic partial charges[64]. All file conversions were performed using the open source chemical toolbox Open Babel 2.3.2 [65]. The

ligand and protein structures were optimised using AutoDock Tools software (AutoDock 1.5.6) which involved adding all hydrogen atoms to the macromolecule, which is a step necessary for correct calculation of partial atomic charges. Gasteiger charges are calculated for each atom of the macromolecule in AutoDock 1.5.6 [64].

NPs were docked against ClpP1P2, DprE1, InhA, KasA, PanK, *P*knB,and Pks13 along with each respective control inhibitors, ZIL (N-[(benzyloxy)carbonyl]-L-isoleucyl-L-leucine), BTZ043, isoniazid, TLM (thiolactomycin), ZVT, MIX, I28. Molecular docking calculations for all compounds with each of the proteins were performed using AutoDock Vina 1.1.2. Docking calculation was generated with the software free energy binding own scoring function. The binding affinity of the ligand was expressed in kcal.mol^{-1}. Nine different poses were calculated for each protein with the parameters num_modes = 9 and exhaustiveness = 16. The lowest energy conformation was chosen for binding model analysis. Molecular interactions between ligand and protein were generated and analysed by LigPlot^{+} and depicted by PyMOL. PyMOL Molecular Graphics System, Version 2.0 Schrödinger (http://www.pymol.org) was used to prepare the Figures.

To provide enough space for free movements of the ligands, the grid box was constructed to cover the active sites as defined using AutoDock 1.5.6. The grid points for ClpP1P2 were set to 18 × 20 × 12, at a grid center of (x,y,z) -84.697, -2.336, 38.022 with spacing of 1 Å. For DprE1, the grid points were set to 20 × 20 × 20, at a grid center of (x,y,z) 14.99, -20.507, 37.226 with spacing of 1 Å. For InhA, the grid points were set to 26 × 24 × 22, at a grid center of (x,y,z) -5.111, 33.222, 13.410 with space ng of 1 Å. For KasA, the grid points were set to 20 × 20 × 20, at a grid center of (x,y,z) 38.342, -7.033, 13.410 with spacing of 1 Å. For PanK, the grid points were set to 20 × 20 × 20, at a grid center of (x,y,z) -18.742, 13.919, 11.679 with spacing of 1 Å. For PknB, the grid points were set to 21 × 20 × 20, at a grid center of (x,y,z) 61.518, 2.429, -25.588 with spacing of 1 Å. For Pks13 the grid points were set to 16 × 18 × 14, at a grid center of (x,y,z) 3.954, 27.324, 8.499 with spacing of 1 Å.

References

1. WHO. *Global tuberculosis report 2018*. (WHO Press, Geneva, 2018).
2. Baptista, R., Bhowmick, S., Nash, R. J., Baillie, L. & Mur, L. A. Target discovery focused approaches to overcome bottlenecks in the exploitation of antimycobacterial natural products. *Future Med. Chem.* **10**, 811–822 (2018).
3. Gupta, V. K., Kumar, M. M., Bisht, D. & Kaushik, A. Plants in our combating strategies against *Mycobacterium tuberculosis*: Progress made and obstacles met. *Pharmaceutical Biology* (2017).
4. McConkey, B. J., Sobolev, V. & Edelman, M. The performance of current methods in ligand-protein docking. *Curr. Sci.* (2002).
5. Lou, Z. & Zhang, X. Protein targets for structure-based anti- *Mycobacterium tuberculosis* drug discovery. **1**, 435–442 (2010).
6. Subramani, R., Narayanasamy, M. & Feussner, K. D. Plant-derived antimicrobials to fight against multi-drug-resistant human pathogens. *3 Biotech* (2017).
7. Espinoza-Moraga, M., Njuguna, N. M., Mugumbate, G., Caballero, J. & Chibale, K. *In silico* comparison of antimycobacterial natural products with known antituberculosis drugs. *J. Chem. Inf. Model.* **53**, 649–660 (2013).
8. Aggarwal, A. *et al.* Development of a novel lead that targets *M. tuberculosis* polyketide synthase 13. *Cell* **170**, 249-259.e25 (2017).
9. Azam, S. S. & Abbasi, S. W. Molecular docking studies for the identification of novel melatoninergic inhibitors for acetylserotonin-O-methyltransferase using different docking routines. *Theor. Biol. Med. Model.* **10**, 63 (2013).
10. Seyedi, S. S. *et al.* Computational approach towards exploring potential anti-chikungunya activity of selected flavonoids. *Sci. Rep.* **6**, 24027 (2016).
11. Qiu, J.-X. *et al.* Estimation of the binding modes with important human cytochrome P450 enzymes, drug interaction potential, pharmacokinetics, and hepatotoxicity of ginger components using molecular docking, computational, and pharmacokinetic modeling studies. *Drug Des. Devel. Ther.* **9**, 841–866 (2015).

12. Natarajan, A., Sugumar, S., Bitragunta, S. & Balasubramanyan, N. Molecular docking studies of (4Z, 12Z)-cyclopentadeca-4, 12-dienone from *Grewia hirsuta* with some targets related to type 2 diabetes. *BMC Complement. Altern. Med.* **15**, 73 (2015).

13. Ali, M. T., Blicharska, N., Shilpi, J. A. & Seidel, V. Investigation of the anti-TB potential of selected propolis constituents using a molecular docking approach. *Sci. Rep.* **8**, 12238 (2018).

14. Raju, R. M. *et al. Mycobacterium tuberculosis* ClpP1 and ClpP2 function together in protein degradation and are required for viability *in vitro* and during infection. *PLoS Pathog.* (2012).

15. Wolucka, B. A. Biosynthesis of D-arabinose in mycobacteria - A novel bacterial pathway with implications for antimycobacterial therapy. *FEBS Journal* (2008).

16. Crellin, P. K., Brammananth, R. & Coppel, R. L. Decaprenylphosphoryl-β-D-Ribose 2′-epimerase, the target of benzothiazinones and dinitrobenzamides, is an essential enzyme in Mycobacterium smegmatis. *PLoS One* (2011).

17. Schaeffer, M. L. *et al.* Purification and biochemical characterization of the mycobacterium tuberculosis β-ketoacyl-acyl carrier protein synthases KasA and KasB. *J. Biol. Chem.* (2001).

18. Das, S., Kumar, P., Bhor, V., Surolia, A. & Vijayan, M. Invariance and variability in bacterial PanK: A study based on the crystal structure of *Mycobacterium tuberculosis* PanK. *Acta Crystallogr. Sect. D Biol. Crystallogr.* (2006).

19. Chawla, Y. *et al.* Protein kinase B (PknB) of *Mycobacterium tuberculosis* is essential for growth of the pathogen in vitro as well as for survival within the host. *J. Biol. Chem.* (2014).

20. Portevin, D. *et al.* A polyketide synthase catalyzes the last condensation step of mycolic acid biosynthesis in mycobacteria and related organisms. *Proc. Natl. Acad. Sci.* (2004) doi:10.1073/pnas.0305439101.

21. Sureram, S. *et al.* Antimycobacterial activity of bisbenzylisoquinoline alkaloids from *Tiliacora triandra* against multidrug-resistant isolates of *Mycobacterium tuberculosis*. *Bioorg. Med. Chem. Lett.* **22**, 2902–2905 (2012).

22. Wehenkel, A. *et al.* The structure of PknB in complex with mitoxantrone, an ATP-competitive inhibitor, suggests a mode of protein kinase regulation in mycobacteria. *FEBS Lett.* **580**, 3018–3022 (2006).

23. Bhutani, I., Loharch, S., Gupta, P., Madathil, R. & Parkesh, R. Structure, dynamics, and interaction of *Mycobacterium tuberculosis* (Mtb) DprE1 and DprE2 examined by molecular modeling, simulation, and electrostatic studies. *PLoS One* **10**, e0119771 (2015).

24. De Pascoli, I. C., Nascimento, I. R. & Lopes, L. M. X. Configurational analysis of cubebins and bicubebin from *Aristolochia lagesiana* and *Aristolochia pubescens*. *Phytochemistry* (2006).

25. Nascimento, I. R., Murata, A. T., Bortoli, S. A. & Lopes, L. M. X. Insecticidal activity of chemical constituents from *Aristolochia pubescens* against *Anticarsia gemmatalis* larvae. *Pest Manag. Sci.* (2004) doi:10.1002/ps.805.

26. Harmatha, J. & Dinan, L. Biological activities of lignans and stilbenoids associated with plant-insect chemical interactions. in *Phytochemistry Reviews* (2003).

27. Jiménez-Arellanes, A. *et al.* Antiprotozoal and antimycobacterial activities of pure compounds from *Aristolochia elegans* rhizomes. *Evidence-based Complement. Altern. Med.* (2012).

28. Esperandim, V. R. *et al.* Evaluation of the *in vivo* therapeutic properties of (−)-cubebin and (−)-hinokinin against *Trypanosoma cruzi*. *Exp. Parasitol.* **133**, 442–446 (2013).

29. Mascarello, A. *et al.* Discovery of *Mycobacterium tuberculosis* Protein Tyrosine Phosphatase B (PtpB) Inhibitors from Natural Products. *PLoS One* **8**, e77081 (2013).

30. Arifullah, M. *et al.* Evaluation of anti-bacterial and anti-oxidant potential of andrographolide and echiodinin isolated from callus culture of *Andrographis paniculata* Nees. *Asian Pac. J. Trop. Biomed.* (2013) doi:10.1016/S2221-1691(13)60123-9.

31. Prabu, A. *et al.* Andrographolide: A potent antituberculosis compound that targets Aminoglycoside 2′-N-acetyltransferase in *Mycobacterium tuberculosis*. *J. Mol. Graph. Model.* (2015) doi:10.1016/j.jmgm.2015.07.001.

32. Navarro-García, V. M., Luna-Herrera, J., Rojas-Bribiesca, M. G., Álvarez-Fitz, P. & Ríos, M. Y. Antibacterial activity of aristolochia brevipes against multidrug-resistant *Mycobacterium tuberculosis*. *Molecules* (2011) doi:10.3390/molecules16097357.

33. León-Díaz, R. *et al.* Antimycobacterial neolignans isolated from *Aristolochia taliscana*. *Mem. Inst. Oswaldo Cruz* (2010) doi:10.1590/S0074-02762010000100006.

34. Jiménez-Arellanes, A. *et al.* Ursolic and oleanolic acids as antimicrobial and immunomodulatory compounds for tuberculosis treatment. *BMC Complement. Altern. Med.* (2013) doi:10.1186/1472-6882-13-258.

35. Jyoti, M. A. *et al.* Antimycobacterial activity of methanolic plant extract of *Artemisia capillaris* containing ursolic acid and hydroquinone against *Mycobacterium tuberculosis*. *J. Infect. Chemother.* (2016) doi:10.1016/j.jiac.2015.11.014.

36. Molina-Salinas, G. M. *et al.* Bioactive metabolites from the Andean flora. Antituberculosis activity of natural and semisynthetic azorellane and mulinane diterpenoids. *Phytochem. Rev.* (2010) doi:10.1007/s11101-010-9162-4.

37. Chen, J. J. *et al.* Novel epoxyfuranoid lignans and antitubercular constituents from the leaves of *Beilschmiedia tsangii*. *Planta Med.* (2007) doi:10.1055/s-2007-967195.

38. Aponte, J. C. *et al.* Anti-infective and cytotoxic compounds present in *Blepharodon nitidum.* *Planta Med.* (2008) doi:10.1055/s-2008-1034330.

39. Mehta, A., Srivastva, G., Kachhwaha, S., Sharma, M. & Kothari, S. L. Antimycobacterial activity of *Citrullus colocynthis* (L.) Schrad. against drug sensitive and drug resistant *Mycobacterium tuberculosis* and MOTT clinical isolates. *J. Ethnopharmacol.* (2013) doi:10.1016/j.jep.2013.06.022.

40. Rojas, R. *et al.* Aegicerin, the first oleanane triterpene with wide-ranging antimycobacterial activity, isolated from *Clavija procera*. *J. Nat. Prod.* (2006) doi:10.1021/np050554l.

41. Changtam, C., Hongmanee, P. & Suksamrarn, A. Isoxazole analogs of curcuminoids with highly potent multidrug-resistant antimycobacterial activity. *Eur. J. Med. Chem.* (2010) doi:10.1016/j.ejmech.2010.07.003.

42. Uc-Cachón, A. H. *et al.* Naphthoquinones isolated from *Diospyros anisandra* exhibit potent activity against pan-resistant first-line drugs *Mycobacterium tuberculosis* strains. *Pulm. Pharmacol. Ther.* (2014) doi:10.1016/j.pupt.2013.08.001.

43. Dey, D., Ray, R. & Hazra, B. Antitubercular and antibacterial activity of quinonoid natural products against multi-drug resistant clinical isolates. *Phyther. Res.* (2014) doi:10.1002/ptr.5090.

44. Lall, N. *et al.* Characterization of intracellular activity of antitubercular constituents from the roots of Eu*clea natalensis. Pharm. Biol.* (2005) doi:10.1080/13880200590951829.

45. van der Kooy, F., Meyer, J. J. M. & Lall, N. Antimycobacterial activity and possible mode of action of newly isolated neodiospyrin and other naphthoquinones from *Euclea natalensis. South African J. Bot.* (2006) doi:10.1016/j.sajb.2005.09.009.

46. Al-Yahya, M. A., Muhammad, I., Mirza, H. H. & El-Feraly, F. S. Antibacterial constituents from the rhizomes of *Ferula communis. Phyther. Res.* (1998) doi:10.1002/(SICI)1099-1573(199808)12:5<335::AID-PTR306>3.0.CO;2-H.

47. Gupta, V. K., Kumar, M. M., Bisht, D. & Kaushik, A. Plants in our combating strategies against *Mycobacterium tuberculosi*s: Progress made and obstacles met. *Pharmaceutical Biology* (2017) doi:10.1080/13880209.2017.1309440.

48. Gordien, A. Y., Gray, A. I., Franzblau, S. G. & Seidel, V. Antimycobacterial terpenoids from *Juniperus communis* L. (Cuppressaceae). *J. Ethnopharmacol.* (2009) doi:10.1016/j.jep.2009.09.007.

49. Mossa, J. S., El-Feraly, F. S. & Muhammad, I. Antimycobacterial constituents from *Juniperus procera, Ferula communis* and *Plumbago zeylanica* and their *in vitro* synergistic activity with isonicotinic acid hydrazide. *Phyther. Res.* (2004) doi:10.1002/ptr.1420.

50. Lakshmanan, D. *et al.* Ethyl p-methoxycinnamate isolated from a traditional anti-tuberculosis medicinal herb inhibits drug resistant strains of *Mycobacterium tuberculosis in vitro. Fitoterapia* (2011) doi:10.1016/j.fitote.2011.03.006.

51. Jiménez-Arellanes, A., Meckes, M., Torres, J. & Luna-Herrera, J. Antimycobacterial triterpenoids from *Lantana hispida* (Verbenaceae). *J. Ethnopharmacol.* (2007) doi:10.1016/j.jep.2006.11.033.

52. Favela-Hernández, J. M. J., García, A., Garza-González, E., Rivas-Galindo, V. M. & Camacho-Corona, M. R. Antibacterial and antimycobacterial lignans and flavonoids from L*arrea tridentata*. *Phyther. Res.* (2012) doi:10.1002/ptr.4660.

53. Rijo, P. *et al.* Antimycobacterial metabolites from *Plectranthus*: Royleanone derivatives against *Mycobacterium tuberculosis* strains. *Chem. Biodivers.* (2010)

doi:10.1002/cbdv.200900099.

54. Kumar, P. *et al.* Anti-mycobacterial activity of plumericin and isoplumericin against MDR M*ycobacterium tuberculosis. Pulm. Pharmacol. Ther.* (2013) doi:10.1016/j.pupt.2013.01.003.

55. Leitão, F. *et al.* Medicinal plants from open-air markets in the State of Rio de Janeiro, Brazil as a potential source of new antimycobacterial agents. *J. Ethnopharmacol.* (2013) doi:10.1016/j.jep.2013.07.009.

56. Gupta, S., Dwivedi, G. R., Darokar, M. P. & Srivastava, S. K. Antimycobacterial activity of fractions and isolated compounds from *Vetiveria zizanioides*. *Med. Chem. Res.* (2012) doi:10.1007/s00044-011-9639-8.

57. Schmitz, K. R., Carney, D. W., Sello, J. K. & Sauer, R. T. Crystal structure of *Mycobacterium tuberculosis* ClpP1P2 suggests a model for peptidase activation by AAA+ partner binding and substrate delivery. *Proc. Natl. Acad. Sci. U. S. A.* **111**, E4587-95 (2014).

58. Richter, A. *et al.* Novel insight into the reaction of nitro, nitroso and hydroxylamino benzothiazinones and of benzoxacinones with *Mycobacterium tuberculosis* DprE1. *Sci. Rep.* **8**, 13473 (2018).

59. Dessen, A., Quemard, A., Blanchard, J., Jacobs, W. & Sacchettini, J. Crystal structure and function of the isoniazid target of *Mycobacterium tuberculosis. Science (80-.).* **267**, 1638–1641 (1995).

60. Luckner, S. R., Machutta, C. A., Tonge, P. J. & Kisker, C. Crystal structures of *Mycobacterium tuberculosis* KasA show mode of action within cell wall biosynthesis and its inhibition by thiolactomycin. *Structure* **17**, 1004–1013 (2009).

61. Bjorkelid, C. *et al.* Structural and biochemical characterization of compounds inhibiting *Mycobacterium tuberculosis* pantothenate kinase. *J. Biol. Chem.* **288**, 18260–18270 (2013).

62. Yap, C. W. PaDEL-descriptor: an open source software to calculate molecular descriptors and fingerprints. *J. Comput. Chem.* **32**, 1466–1474 (2011).

63. Chong, J. *et al.* MetaboAnalyst 4.0: towards more transparent and integrative metabolomics analysis. *Nucleic Acids Res.* **46**, W486–W494 (2018).

64. Umamaheswari, M. *et al. In silico* docking studies of aldose reductase inhibitory activity of

selected flavonoids. *Int. J. Drug Dev. Res.* (2012).

65. O'Boyle, N. M. *et al.* Open Babel: An Open chemical toolbox. *J. Cheminform.* (2011).

Acknowledgments

R.B. was supported by a Natural Life Sciences Research Network PhD Scholarship. S.B. is thankful to Aberystwyth University for its AberDoc PhD Scholarship. The authors have no other relevant affiliations or financial involvement with any organization or entity with a financial interest in or financial conflict with the subject matter or materials discussed in the manuscript apart from those disclosed. No writing assistance was utilised in the production of this manuscript.

Author Contributions

R.B., S.B. J.S. and L.A.J.M. conceived and designed the study. R.B. and S.B. performed the computational studies. R.B. analysed the data and prepared the figures. R.B., S.B. J.S. and L.A.J.M. wrote the paper. All authors reviewed the manuscript.

Supplementary Figures

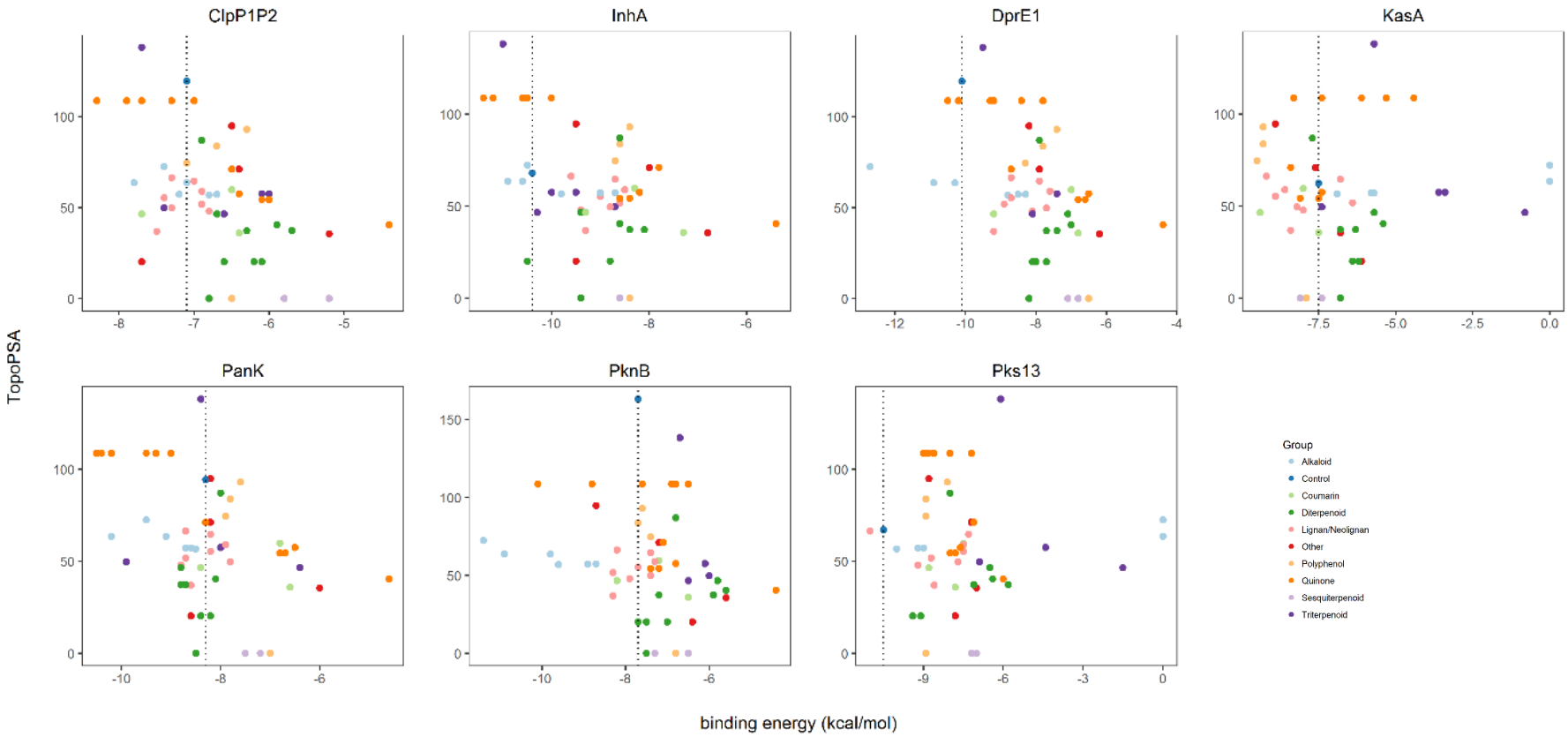

Supplementary Figure 1 – Topological polar surface (TopoPSA) and binding energy of studied natural products against ClpP1P2, DprE1, InhA, KasA, PanK, PknB and Pks13.

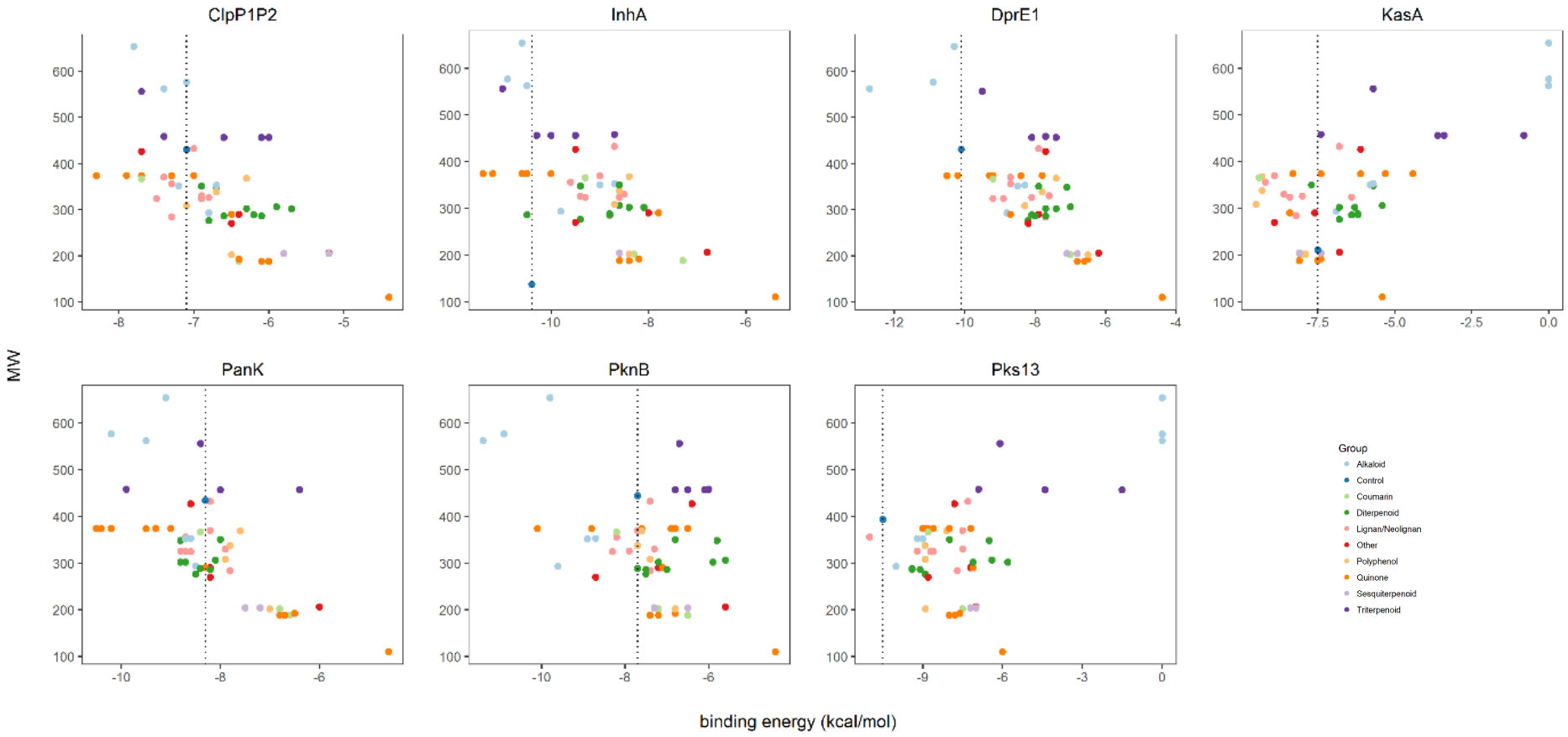

Supplementary Figure 2 – Molecular weight (MW) and binding energy of studied natural products against ClpP1P2, DprE1, InhA, KasA, PanK, PknB and Pks13.

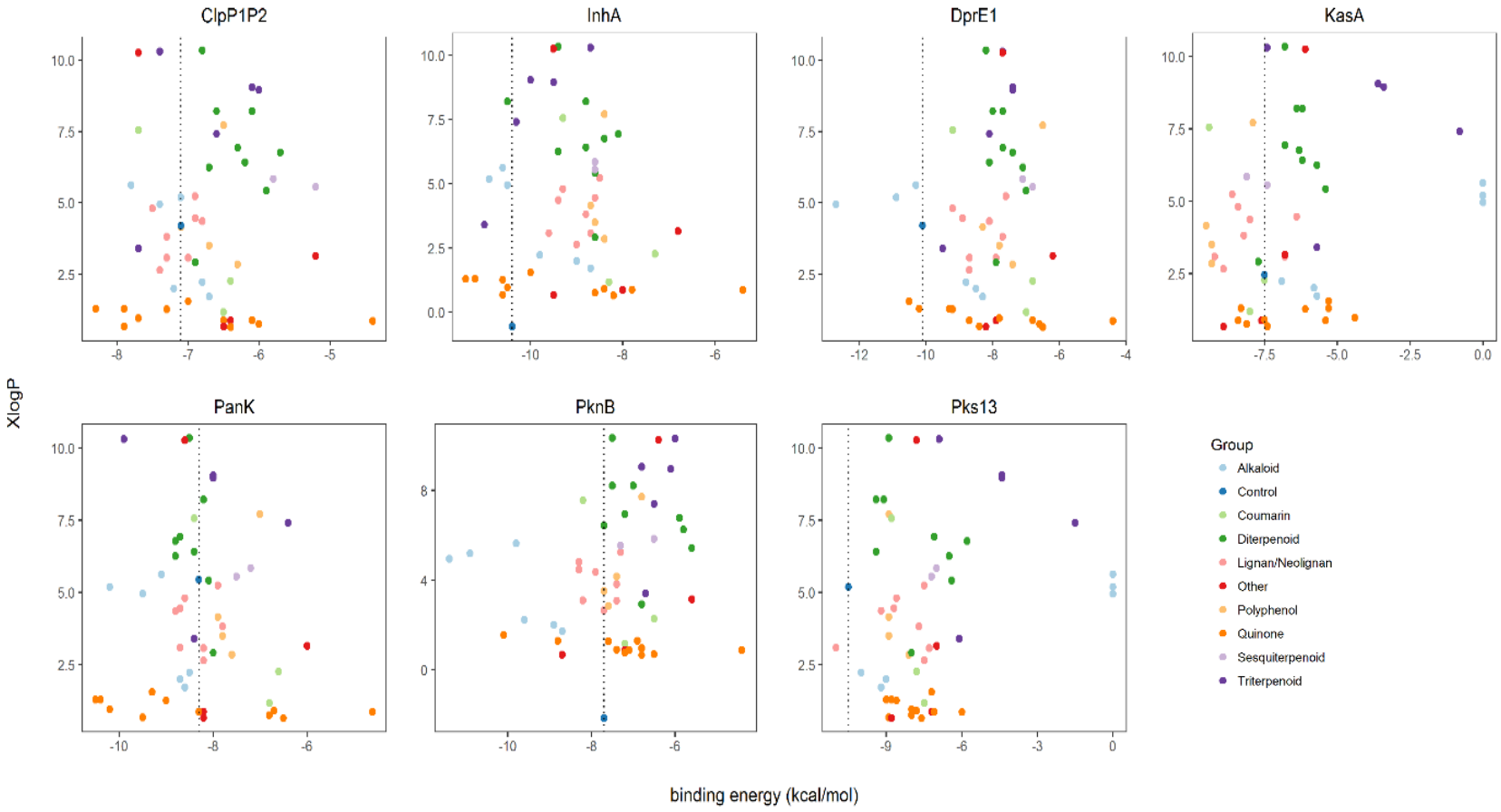

Supplementary Figure 3 – Partition coefficient (XLogP) and binding energy of studied natural products against ClpP1P2, DprE1, InhA, KasA, PanK, PknB and Pks13.

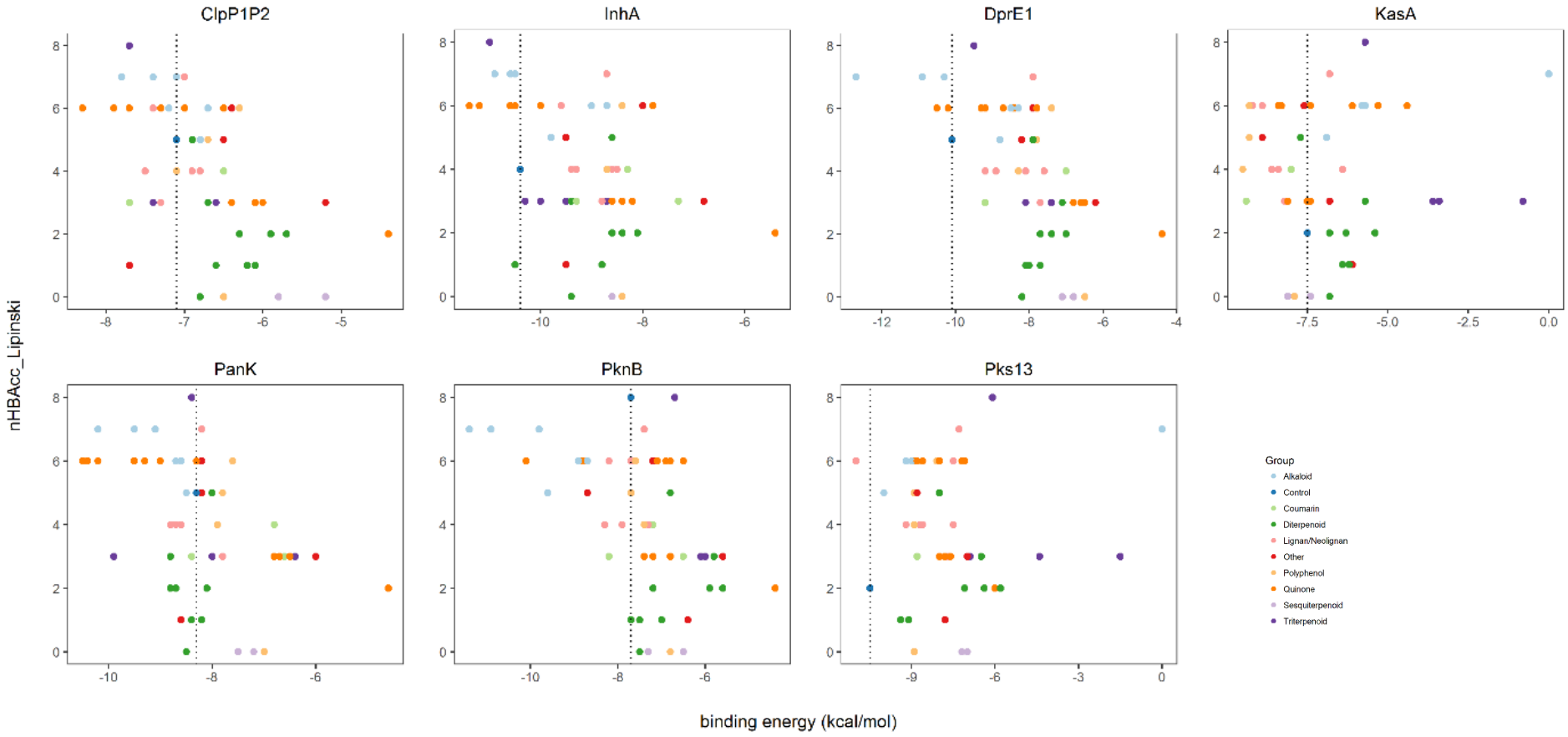

Supplementary Figure 4 – Number of H-bonds acceptors (nHBAcc_Lipinski) and binding energy of studied natural products against ClpP1P2, DprE1, InhA, KasA, PanK, PknB and Pks13.

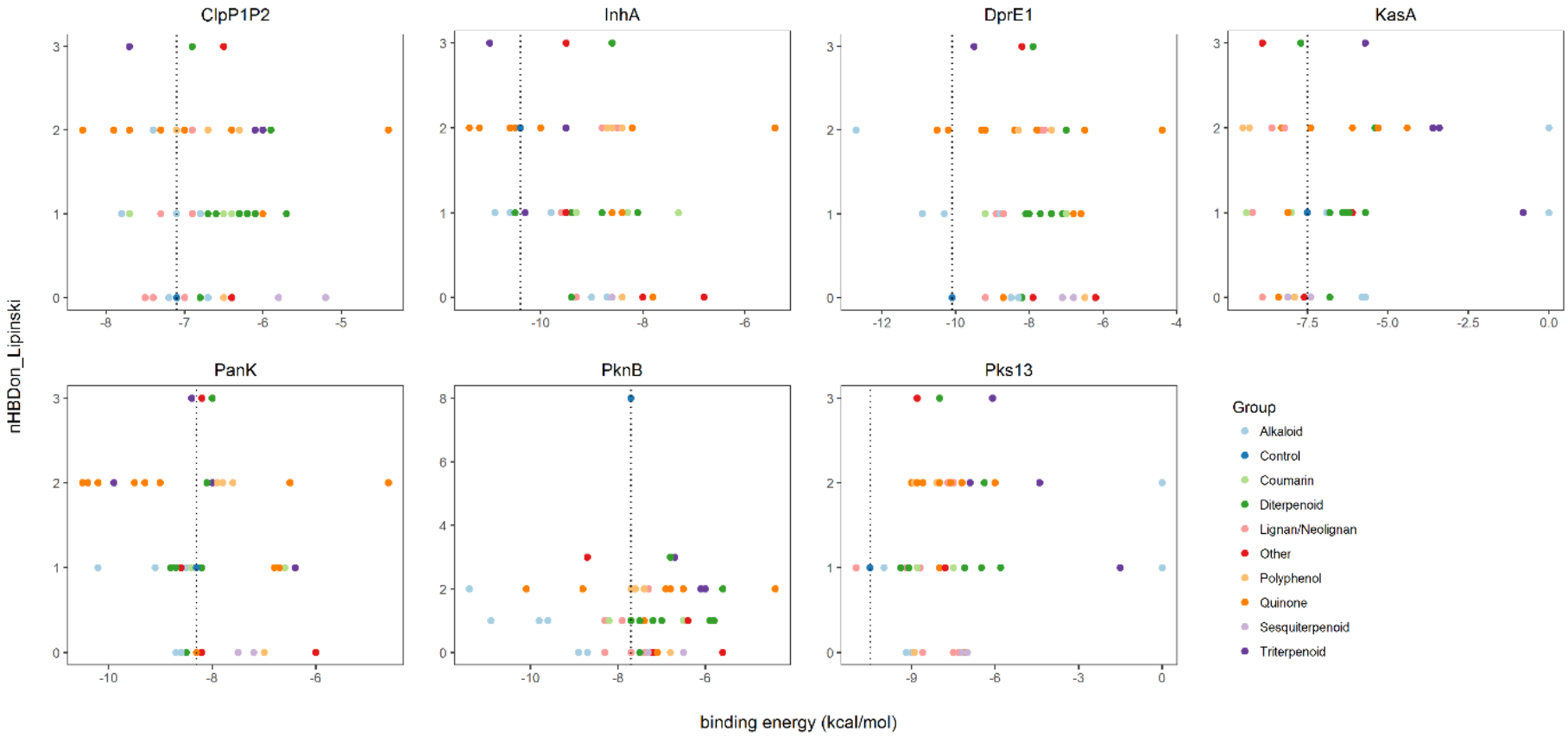

Supplementary Figure 5 – Number of H-bonds donnors (nHBDon_Lipinski) and binding energy of studied natural products against ClpP1P2, DprE1, InhA, KasA, PanK, PknB and Pks13.

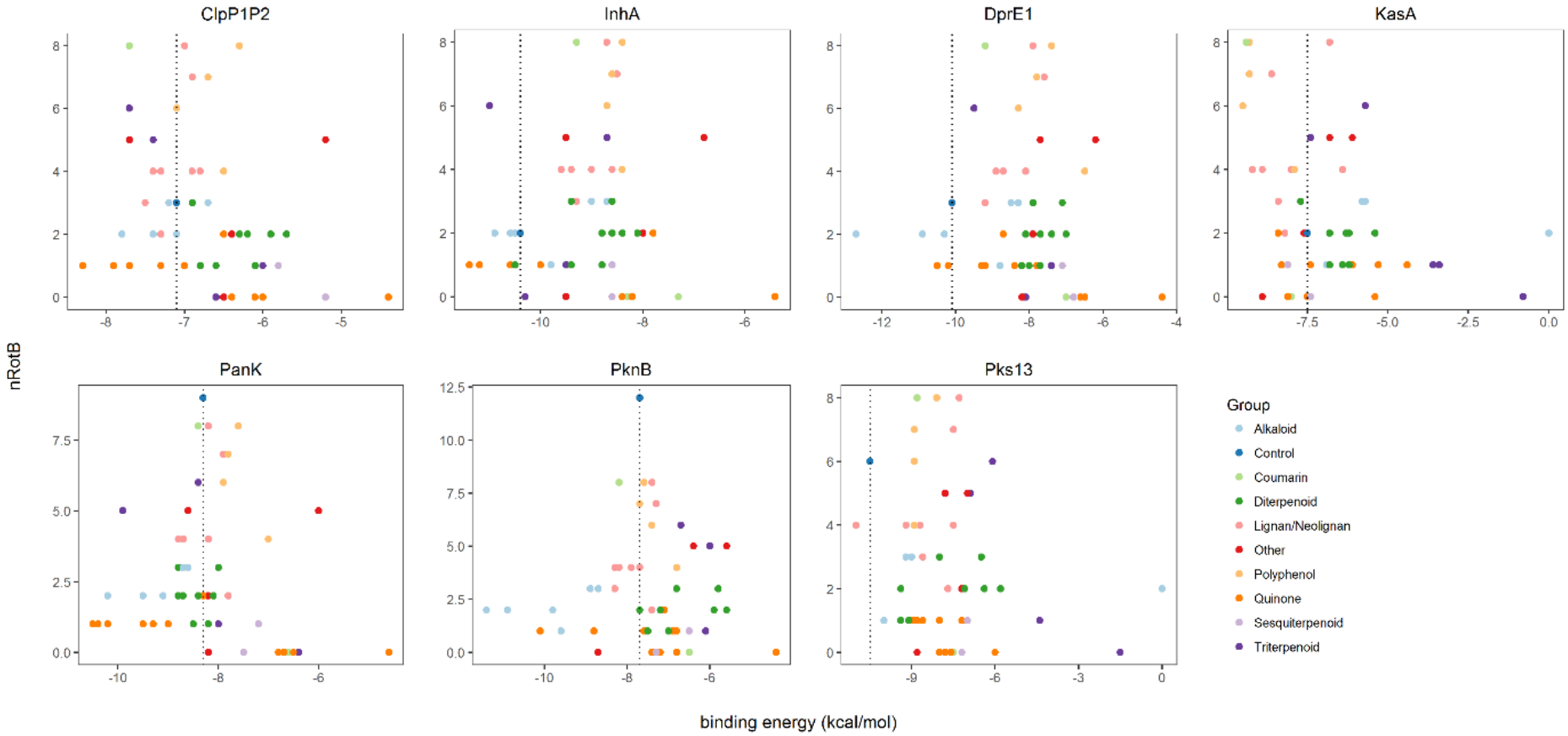

Supplementary Figure 6 – Number of rotational bonds (nRotB) and binding energy of studied natural products against ClpP1P2, DprE1, InhA, KasA, PanK, PknB and Pks13.

1 Supplementary Table 1

	Group	Name	nHBAcc_Lipinski	nHBDon_Lipinski	nRotB	TopoPSA	MW	XLogP	Pks13	PknB	PanK	KasA	InhA	DprE1	ClpP1P2
Licarin A	Lignan/Neolignan	1	4	1	4	48	326	4.36	-9	-8	-9	-8	-9.4	-8.1	-6.8
Licarin B	Lignan/Neolignan	2	4	0	3	37	324	4.81	-9	-8	-9	-8.4	-9.3	-9.2	-7.5
eupomatenoid-7	Lignan/Neolignan	3	4	1	4	52	324	4.46	-9	-8	-9	-6.4	-8.6	-8.9	-6.9
Aristolactam I	Alkaloid	4	5	1	1	57	293	2.23	-10	-10	-9	-6.9	-9.8	-8.8	-6.8
Fargesin	Neolignan	5	6	0	4	55	370	2.65	-8	-8	-8	-8.9	-9	-8.7	-7.4
alpha-Cubebin	Lignan/Neolignan	6	6	1	4	66	356	3.08	-11	-8	-9	-9.2	-9.6	-8.7	-7.3
Ursolic acid	Triterpenoid	7	3	2	1	58	456	8.95	-4	-6	-8	-3.4	-9.5	-7.4	-6
Hydroquinone	Quinone	8	2	2	0	40	110	0.87	-6	-4	-5	-5.4	-5.4	-4.4	-4.4
azorellanol	Diterpenoid	9	3	1	3	47	348	6.25	-7	-6	-9	-5.7	-9.4	-7.1	-6.7
Beilschmin A	Lignan/Neolignan	10	7	0	8	65	432	3.08	-7	-7	-8	-6.8	-8.7	-7.9	-7
25-Hydroperoxycycloart-23-en-3beta-ol	Triterpenoid	11	3	2	5	50	458	10.3	-7	-6	-10	-7.4	-8.7	-7.7	-7.4
cucurbitacin E	Triterpenoid	12	8	3	6	138	556	3.4	-6	-7	-8	-5.7	-11	-9.5	-7.7
aegicerin	Triterpenoid	13	3	1	0	47	456	7.41	-2	-7	-6	-0.8	-10.3	-8.1	-6.6
Diospyrin	Quinone	14	6	2	1	109	374	1.29	-9	-9	-10	-8.3	-11.2	-9.3	-8.3
5-Hydroxy furanocoumarin or bergaptol	Coumarin	15	4	1	0	60	202	1.17	-8	-7	-7	-8	-8.3	-7	-6.5
vasicine	Coumarin	16	3	1	0	36	188	2.27	-8	-7	-7	-7.5	-7.3	-6.8	-6.4
Ethyl 4-Methoxycinnamate	Other	17	3	0	5	36	206	3.15	-7	-6	-6	-6.8	-6.8	-6.2	-5.2
Oleanolic acid	Triterpenoid	18	3	2	1	58	456	9.05	-4	-7	-8	-3.6	-10	-7.4	-6.1
Dihydroguaiaretic acid	Lignan/Neolignan	19	4	2	7	59	330	5.24	-8	-7	-8	-8.6	-8.5	-7.6	-6.9

4-Epi-larreatricin	Lignan/Neolignan	20	3	2	2	50	284	3.82	-8	-7	-8	-8.2	-8.8	-7.7	-7.3
Abietane	Diterpenoid	21	0	0	1	0	276	10.3	-9	-8	-9	-6.8	-9.4	-8.2	-6.8
Plumericin	Other	22	6	0	2	71	290	0.88	-7	-7	-8	-7.6	-8	-7.9	-6.4
Tiliacorinine	Alkaloid	24	7	2	2	72	562	4.95	3.7	-11	-10	32.7	-10.5	-13	-7.4
2'-Nortiliacorinine	Alkaloid	25	7	1	2	64	576	5.19	1.4	-11	-10	28.3	-10.9	-11	-7.1
Plumbagin	Quinone	26	3	1	0	54	188	0.76	-8	-7	-7	-8.1	-8.6	-6.6	-6
Maritinone or 8,8’-biplumbagin	Quinone	27	6	2	1	109	374	0.68	-9	-7	-10	-7.4	-10.6	-8.4	-7.9
3,3’-biplumbagin	Quinone	28	6	2	1	109	374	1.27	-9	-8	-9	-6.1	-10.6	-9.2	-7.3
6?-7-dehydro-N formyl-nornantenine	Alkaloid	29	6	0	3	57	351	2	-9	-9	-9	-5.8	-9	-8.5	-7.2
N-formylnornantenine	Alkaloid	30	6	0	3	57	353	1.72	-9	-9	-9	-5.7	-8.7	-8.3	-6.7
Mulin-11,13-dien-20-oic acid	Diterpenoid	31	2	1	2	37	302	6.77	-6	-6	-9	-6.3	-8.4	-7.4	-5.7
Mulinol	Diterpenoid	32	2	2	2	40	306	5.42	-6	-6	-8	-5.4	-8.6	-7	-5.9
Curcumin	Polyphenol	35	6	2	8	93	368	2.85	-8	-8	-8	-9.3	-8.4	-7.4	-6.3
demethoxycurcumin	Polyphenol	36	5	2	7	84	338	3.5	-9	-8	-8	-9.3	-8.6	-7.8	-6.7
bisdemethoxycurcumin	Polyphenol	37	4	2	6	75	308	4.16	-9	-7	-8	-9.5	-8.7	-8.3	-7.1
Isodiospyrin	Quinone	38	6	2	1	109	374	0.96	-8	-7	-10	-4.4	-10.5	-7.8	-7.7
Mamegakinone	Quinone	39	6	2	1	109	374	1.55	-7	-10	-9	-5.3	-10	-11	-7
7-methyljuglone	Quinone	40	3	1	0	54	188	0.9	-8	-7	-7	-7.5	-8.4	-6.8	-6.1
Neodiospyrin	Quinone	41	6	2	1	109	374	1.29	-9	-7	-11	-5.3	-11.4	-10	-7.9
Shinanolone	Quinone	42	3	2	0	58	192	0.65	-8	-7	-7	-7.4	-8.2	-6.5	-6.4
isoplumericin	Quinone	46	6	0	2	71	290	0.88	-7	-7	-8	-8.4	-7.8	-8.7	-6.5
13?-bromo-tiliacorinine	Alkaloid	47	7	1	2	64	654	5.63	4.6	-10	-9	52.3	-10.6	-10	-7.8
a-curcumene	Polyphenol	49	0	0	4	0	202	7.71	-9	-7	-7	-7.9	-8.4	-6.5	-6.5
valencene	Sesquiterpenoid	50	0	0	1	0	204	5.85	-7	-7	-7	-8.1	-8.6	-7.1	-5.8
Selina-3,7(11)-diene	Sesquiterpenoid	51	0	0	0	0	204	5.55	-7	-7	-8	-7.4	-8.6	-6.8	-5.2
Emodin	Other	52	5	3	0	95	270	0.66	-9	-9	-8	-8.9	-9.5	-8.2	-6.5
Andrographolide	Diterpenoid	53	5	3	3	87	350	2.91	-8	-7	-8	-7.7	-8.6	-7.9	-6.9
Obtusifoliol	Other	54	1	1	5	20	426	10.3	-8	-6	-9	-6.1	-9.5	-7.7	-7.7
Totarol	Diterpenoid	55	1	1	1	20	286	8.21	-9	-7	-8	-6.2	-10.5	-7.7	-6.1

Ferruginol	Diterpenoid	56	1	1	1	20	286	8.21	-9	-8	-8	-6.4	-8.8	-8	-6.6
sandaracopimeric acid	Diterpenoid	57	2	1	2	37	302	6.94	-7	-7	-9	-6.8	-8.1	-7.7	-6.3
4-Epiabietol	Diterpenoid	58	1	1	2	20	288	6.42	-9	-8	-8	-6.2	-8.8	-8.1	-6.2
ferulenol	Coumarin	59	3	1	8	47	366	7.56	-9	-8	-8	-9.4	-9.3	-9.2	-7.7
	Control	ZIL	7	3	13	105	378	5.05							-7.1
	Control	BTZ043	5	0	3	120	431	4.2						-10	
	Control	I28	2	1	6	67	393	5.19	-11						
	Control	INH	4	2	2	68	137	-0.57					-10.4		
	Control	MIX	8	8	12	163	444	-2.17		-8					
	Control	TLM	2	1	2	63	210	2.46				-7.5			
	Control	ZVT	5	1	9	94	434	5.44			-8				

1

2